

We are IntechOpen, the world's leading publisher of Open Access books Built by scientists, for scientists

4,800

Open access books available

122,000

International authors and editors

135M

Downloads

Our authors are among the

154

Countries delivered to

TOP 1%

most cited scientists

12.2%

Contributors from top 500 universities



WEB OF SCIENCE™

Selection of our books indexed in the Book Citation Index
in Web of Science™ Core Collection (BKCI)

Interested in publishing with us?
Contact book.department@intechopen.com

Numbers displayed above are based on latest data collected.
For more information visit www.intechopen.com



Alteration Reaction and Mass Transfer via Fluids with Progress of Fracturing along the Median Tectonic Line, Mie Prefecture, Southwest Japan

Yumi Kaneko, Toru Takeshita, Yuto Watanabe,
Norio Shigematsu and Ko-Ichiro Fujimoto

Additional information is available at the end of the chapter

<http://dx.doi.org/10.5772/68112>

Abstract

We have analyzed mass transfer in the cataclasite samples collected from the Median Tectonic Line, southwest Japan, in which the degree of fracturing is well correlated with the bulk rock chemical compositions determined by the X-ray fluorescence (XRF) analysis. The results of “isocon” analysis indicate not only a large volume increase up to 110% but also the two-stage mass transfer during cataclasis. At the first stage from the very weakly to weakly fractured rocks, the weight percents of SiO₂, Na₂O, and K₂O increase, while those of TiO₂, FeO, MnO, MgO, and CaO decrease. At the second stage from the weakly to moderately and strongly fractured rocks, the trend of mass transfer is reversed. The principal component analysis reveals that the variation of chemical compositions in the cataclasite samples can be mostly interpreted by the mass transfer via fluids and by the difference in chemical composition in the protolith rocks to lesser degree. Finally, the changes in the modal composition of minerals with increasing cataclasis analyzed by the X-ray diffraction (XRD) with the aid of “RockJock” software clearly elucidate that the mass transfer of chemical elements was caused by dissolution and precipitation of minerals via fluids in the cataclasite samples.

Keywords: Median Tectonic Line, cataclasite, mass transfer, isocon analysis, dissolution and precipitation of minerals

1. Introduction

In the Japanese islands, a various scale of faults in different orientations develop as shown by the distribution of active faults (e.g., see [1]), and part of a significant amount strain rate as measured with a global positioning system (GPS) [2] could be explained by a various amount of displacement rate along these faults. Since a lower part of crust underneath the Japanese islands arc is fairly ductile due to a high geothermal gradient, c. 30°C/km, it is only sustained by a thin rigid upper crust of c. 10 km thick (i.e., thin-skinned plate [3]). Therefore, it is very important to elucidate how high the strength (i.e., constitutive equations) along faults is, and how fast the displacement occurs along them in the upper crust, which enables us to discuss about the strain rate and differential stress in the crust, and hence dynamic processes in it.

It has been interpreted that the fault zones, which are originally formed as relatively short narrow segments, are linked to become long faults, and then widen to become mature and weak fault zones [4, 5]. During the fault development, the fault zones formed at the wide depth range above the brittle-ductile transition depth become weakened by frictional sliding along mica or clay minerals with lower internal coefficients of friction accommodated by pressure solution creep (e.g., see [6, 7]), the amount of which increases with increasing deformation aided by alteration of fault rocks [8, 9]. As shown in the present study, new minerals which have different chemical compositions from those of the dissolved minerals and stable under new temperature and pressure conditions precipitate at the dilatant site caused by microfracturing from the solution in cataclasite constituting a fault core (e.g., filling minerals between amphibole microboudine, see [10]). These series of processes could be called dissolution-precipitation creep in a broad sense, in contrast to that in single-phase mineral aggregates studied by many researchers (e.g., see [11]). Hence, to analyze dissolution and precipitation of minerals based on element migration in cataclasite via fluids as conducted in the present study may be equivalent to analyze dissolution-precipitation creep in the broad sense.

In the present research, element migration via fluids in the Cretaceous granitoid cataclasite core samples from the borehole drilled through the Median Tectonic Line (MTL) in Mie Prefecture, southwest Japan [12], has been analyzed. We have first quantified the degree of cataclasis, based on the fracture density (number/cm) measured on the thin sections. Then, we have analyzed altered minerals in both plagioclase and fine-grained materials (ultracataclasite) in the cataclasite samples mostly using a scanning electron microscopy with energy dispersive X-ray spectrometry (SEM-EDS). We further analyzed the bulk rock compositions with an X-ray fluorescence (XRF) and modal composition of minerals constituting the cataclasite samples with an X-ray diffraction (XRD) with the aid of the software "RockJock" [13] as a function of degree of cataclasis. Further, the "isocon" method [14] is employed to analyze the mass transfer in the cataclasite, and further the origin of large variation in chemical composition has been analyzed with the method of principal component analysis (PCA, e.g., see [15]). Finally, we discussed the development of the cataclasite zone along the MTL based on chemical reaction and mass transfer which occurred in this zone.

2. Geological setting and sample description

The MTL (**Figure 1**) was originally formed as the boundary normal fault between the Cretaceous Ryoke granitic and low-P/T type metamorphic rocks, and Cretaceous high-P/T type Sambagawa metamorphic rocks during exhumation of the latter rocks in the earliest Paleogene (c. 60 Ma, e.g., see [16]). In the upper plate consisting of the Ryoke rocks, a shear zone consisting of the so-called the Kashio mylonite was formed in the latest Cretaceous, along which a large amount of sinistral displacement is inferred to have occurred [17–19]. As the time passed, the mylonite zone in the Ryoke rocks, which was developed into the MTL, was overprinted by cataclastic deformation during exhumation and cooling. The Ryoke granitoid cataclasite samples of drill core analyzed in this study are from a borehole drilled by the Geological Survey of Japan, AIST, at the Matsusaka–Iitaka observatory (ITA), Mie Prefecture, Japan. This borehole was drilled through the Median Tectonic Line in Mie Prefecture, southwest Japan, at the depth of 473.9 m and further drilled through the Sambagawa metamorphic rocks down to the depth of 600 m (**Figures 1** and **2**, see [12]). The positions of the MTL at both outcrops and borehole reveal a fault plane orientation of the MTL as N86°E56°N, which is consistent with the attitude of planar fabrics in the gouge zone in direct proximity to the MTL [12, 20]. The protolith of the Ryoke granitoids distributed in this area is mostly tonalite, called Hatai tonalite or Arataki granodiorite [21, 22].

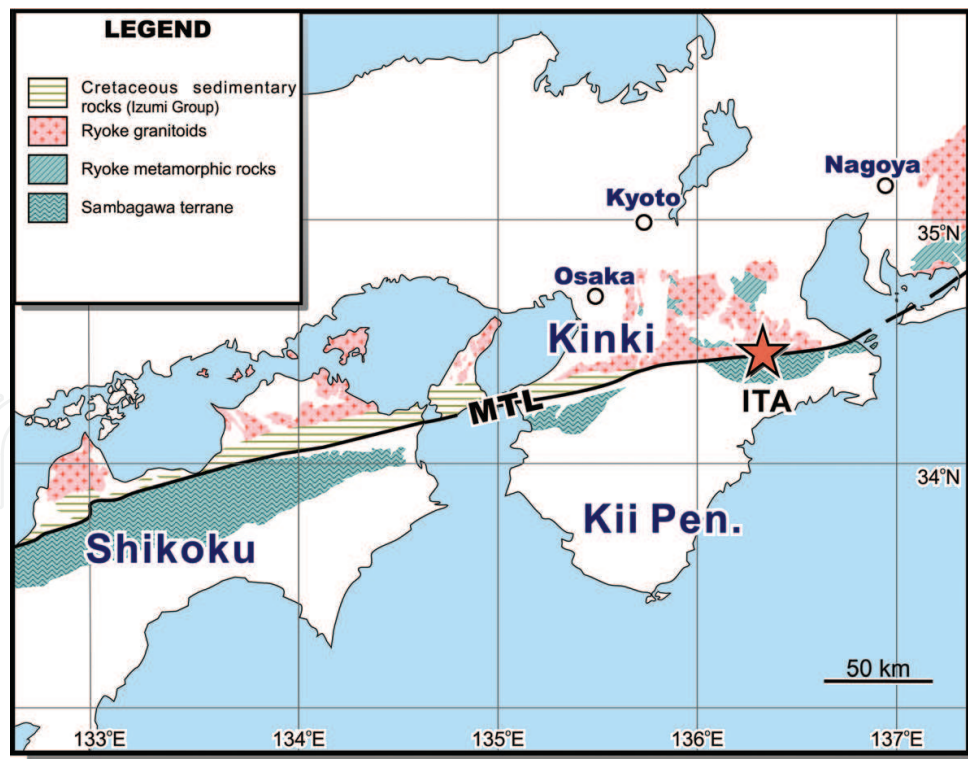


Figure 1. Index map of the Ryoke and Sambagawa belts with the MTL and locality of the Matsusaka-Iitaka (ITA) borehole.

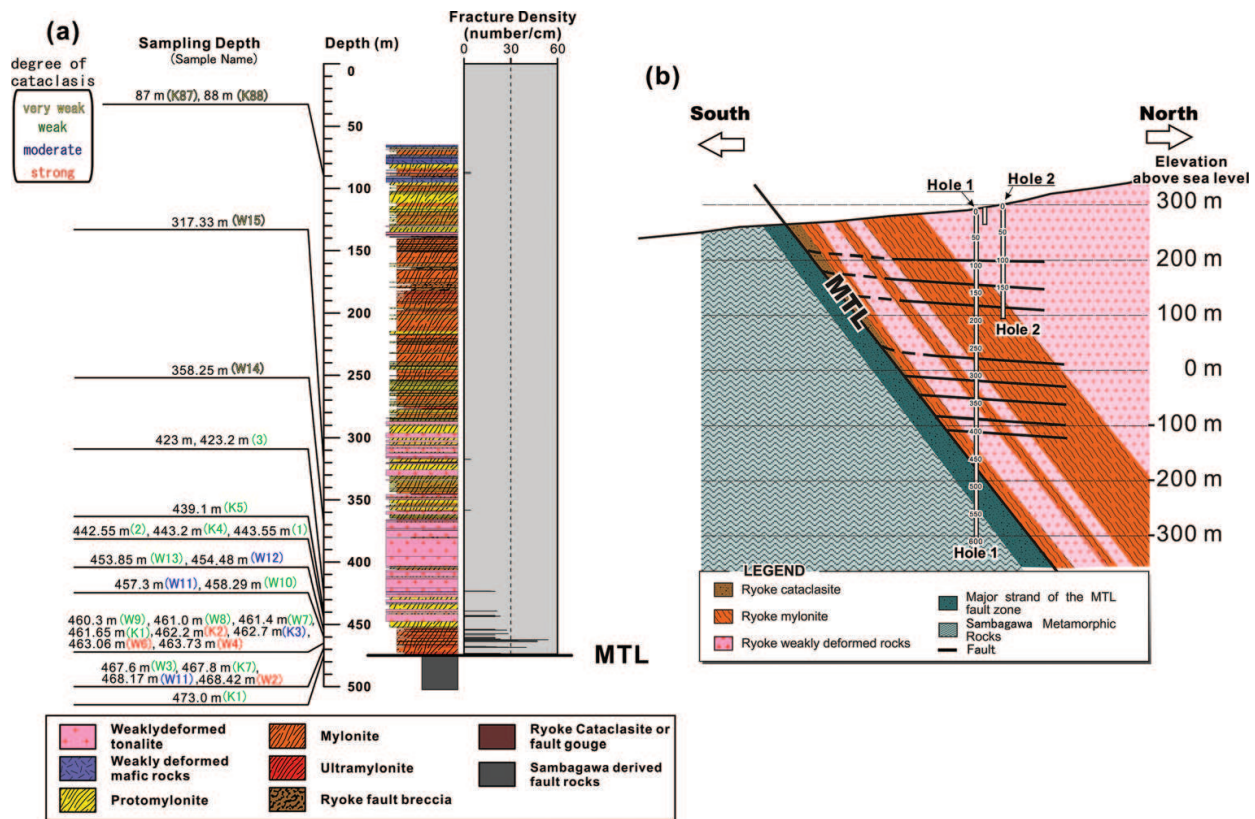


Figure 2. (a) Sample localities of the cataclasite samples in a lithology column of the Matsusaka-Iitaka (ITA) borehole. (b) Cross section of the ITA borehole. Modified after Ref. [12].

3. Results

3.1. Fracture density in the cataclasite

Based on observations of the cataclasite samples by naked eyes, they can be divided into four groups in terms of the degree of cataclasis: very weakly, weakly, moderately and strongly fractured cataclasites (Figure 2). Further, based on observations of some of the cataclasite samples under an optical microscope, the fracture density (FD) is determined to vary for one very weakly (W14; $FD = 4.8/cm$), seven weakly (K13, K14, K7, K5, K4, K11, W3; $FD = 15.7-25.6/cm$), three moderately (K6, K3, W12; $FD = 30.1-37.7/cm$) and two strongly (W2, K2; $FD = 43.9-59.2/cm$) fractured cataclasite (Table 1). It should be noted that non-fractured rocks cannot be found near the cataclasite zone constituting the upper plate of the MTL (Figure 1), and hence the very weakly fractured cataclasite samples collected at the depth of 87, 88, 317 and 358 m should be only considered as a relatively fracture-free samples among the analyzed cataclasite samples.

Microphotographs of these cataclasite samples with different degree of cataclasis are shown in Figure 3. As seen in this figure, in the very weakly fractured cataclasite sample (W14), a mylonite foliation consisting of elongate quartz aggregates is still well preserved, although the plagioclase grains are pervasively sericitized (Figure 3a, b). In the weakly fractured cataclasite sample (W10), although anastomosing fractures along which white mica is grown are pervasively

W14 [#]	W3 ^{\$}	K13 ^{\$}	K14 ^{\$}	K7 ^{\$}	K5 ^{\$}	K4 ^{\$}	K1 ^{\$}	W12 [%]	K6 [%]	K3 [%]	W2 ^{&}	K2 ^{&}
4.83	15.65	17.69	19.83	22.75	23.25	25.58	25.61	30.14	33.92	37.74	43.92	59.19

Table 1. Results for fracture densities in the cataclasite samples. Degree of cataclasis: [#], very weak; ^{\$}, weak; [%], moderate; [&], strong.

developed, the original clasts consisting of stretched quartz aggregates are still preserved (**Figure 3c, d**). In the strongly fractured sample (W4), plagioclase and quartz clasts become very fine grained by strong comminution, and not only white mica, but also chlorite are grown in the fine-grained part (ultracataclasite, **Figure 3e, f**).

3.2. Mineral phases grown in altered plagioclase and fine-grained aggregates (ultracataclasite)

From the observations of thin sections of the cataclasite samples under an optical microscope, it is quite clear that the increase of fracture density (i.e., the degree of cataclasis) is accompanied by the increase of the degree of alteration (i.e., growth of new minerals by metamorphic reaction via fluids, **Figure 3**). Since the comminuted minerals and newly grown minerals are very fine grained, it is very difficult to identify these mineral phase under an optical microscope. Therefore, analysis of microstructures and identification of these fine-grained mineral phases are mostly conducted with a SEM (JSM-5310) and EDS (Oxford-7068). As mentioned below, in weakly to strongly fractured rocks, white mica (phengite, here referred to as muscovite) is grown either replacing original plagioclase altered to albite (weakly fractured Sample K14, **Figure 4a**), or as fracture-filling minerals (i.e., veins, weakly fractured samples W10, **Figure 3c, d**). The existence of white mica is shown by a large amount of both K and Al (**Figure 4a**). In the former sample, prehnite is also grown replacing albite, shown by a large amount of both Ca and Al (**Figure 4a**).

In a strongly fractured cataclasite samples (K2), the fragments of albite and quartz are identified by a large amount of Na, and that of Si alone, respectively (**Figure 4b**). Chlorite shown by a large amount of both Mg and Fe makes an anastomosing network surrounding the fractured plagioclase and quartz. Further, the presence of fine-grained sphene is shown by a large amount of both Ti and Ca. In this sample, both long axis of fractured clasts and grown minerals are aligned in the top-down direction, forming a foliated cataclasite [23].

3.3. Bulk rock composition in the cataclasite samples

Bulk rock composition in the cataclasite samples determined with an XRF analysis is shown in **Table 2**, and also the stratigraphic changes (**Figure 5**) are shown with different colors defined by the different degree of fracturing in the cataclasite samples. Although the compositions in the cataclasite samples with different degree of cataclasis greatly vary, there is a general tendency of variation in the composition with increasing cataclasis, as mentioned below. It is noted, however, that the composition of the protolith tonalite mylonite is not well constrained, because it was not possible to obtain samples free from fractures.

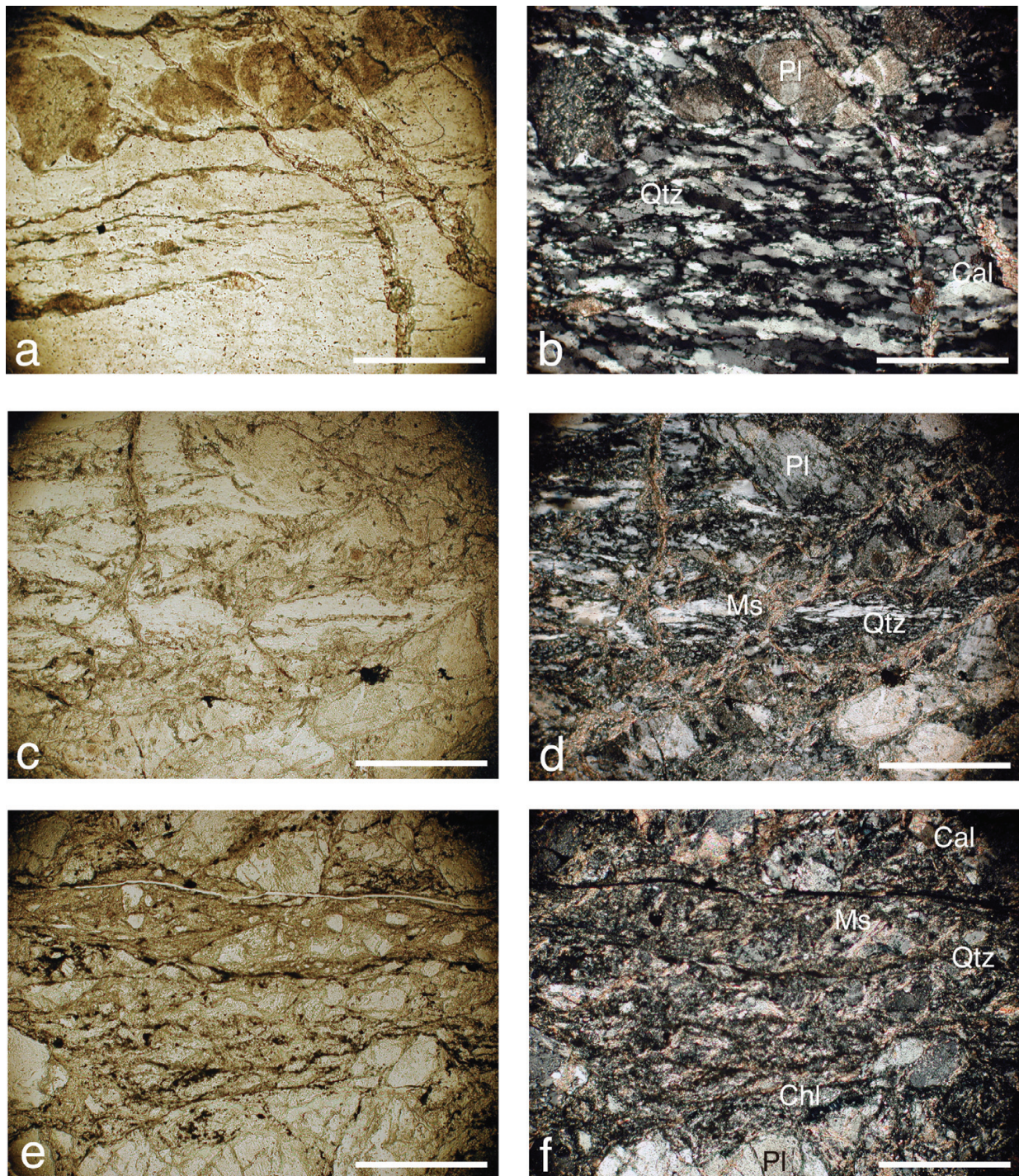


Figure 3. Microphotographs of the cataclasite samples. (a, b) Very weakly fractured sample (W14). (c, d) Weakly fractured sample (W10). (e, f) Strongly fractured sample (W4). (a), (c) and (e) are taken with plane polarized light, while (b), (d) and (f) with crossed polarized light. Scale bars are all 0.4 mm. Abbreviation: Qtz, quartz; Pl, plagioclase; Cal, calcite; Ms, muscovite; Chl, chlorite.

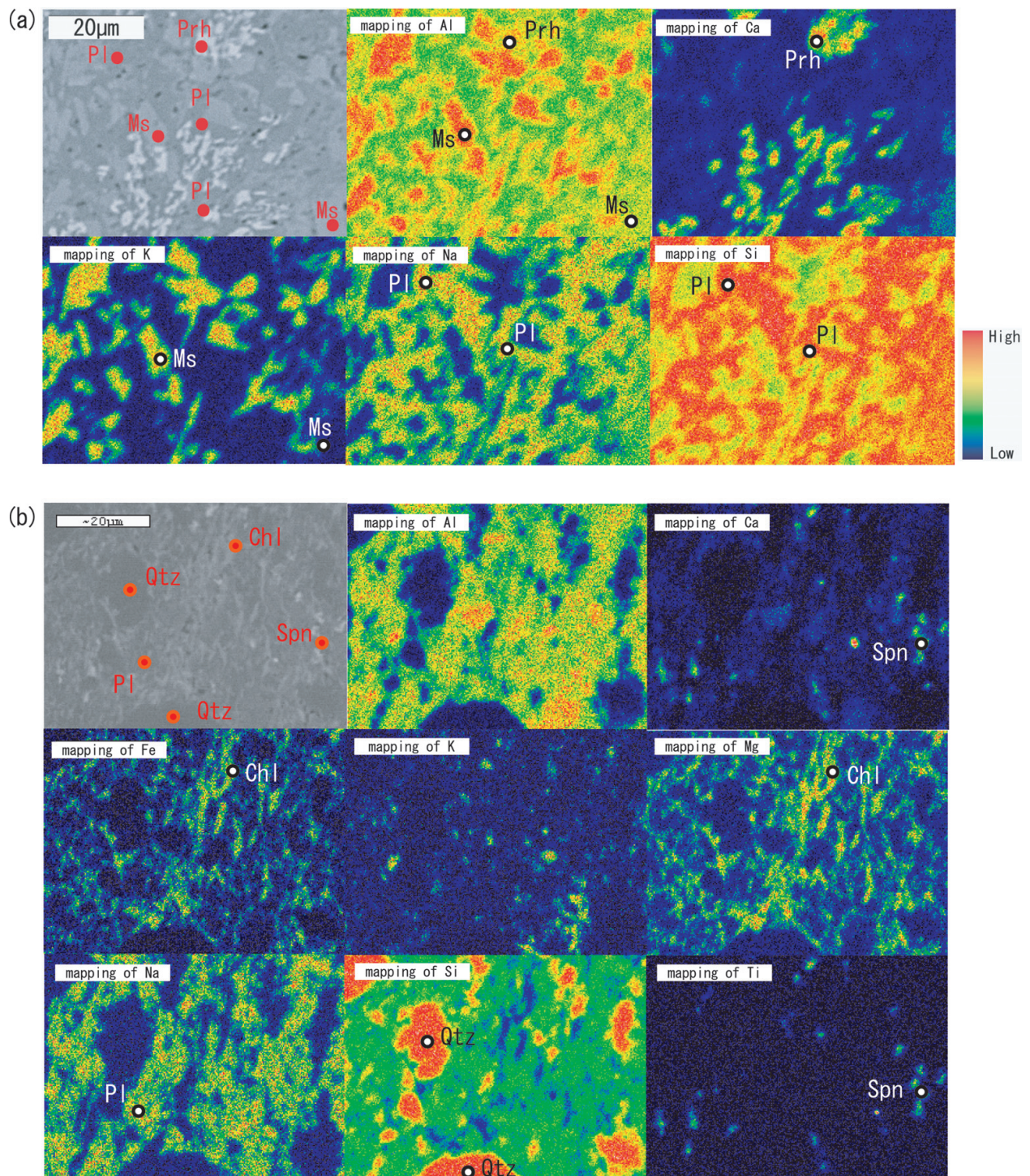


Figure 4. SEM-BSE image and EDS mapping for the cataclasite samples of different degree. See text for explanations. (a) Sample K14 (weakly fractured). (b) Sample K2 (strongly fractured). Abbreviation: Qtz, quartz; Pl, plagioclase; Cal, calcite; Ms, muscovite; Chl, chlorite; Prh, prehnite; Rt, rutile; Spn, sphene.

Oxide (wt%)	W15 [#]	W14 [#]	W13 ^{\$}	W12 [%]	W10 ^{\$}	W9 ^{\$}	W8 ^{\$}	W7 ^{\$}	W6 ^{&}	W5 ^{&}	W4 ^{&}	W2 ^{&}	W1 ^{\$}
SiO ₂	63.81	70.88	72.83	61.82	76.38	69.98	72.90	75.28	50.76	50.16	50.89	55.65	70.85
TiO ₂	0.68	0.30	0.02	0.99	0.11	0.21	0.20	0.09	0.65	0.61	0.63	0.37	0.28
Al ₂ O ₃	17.15	14.70	12.16	15.70	12.53	13.62	13.75	13.23	17.04	17.72	17.90	16.19	14.07
FeO*	4.57	2.40	0.74	4.75	1.15	2.20	2.15	1.13	6.45	5.79	5.95	3.88	2.51
MnO	0.09	0.05	0.02	0.10	0.02	0.05	0.05	0.03	0.14	0.12	0.12	0.10	0.04
MgO	1.86	0.85	0.13	2.38	0.29	0.56	0.46	0.23	6.73	5.39	5.39	4.12	0.84
CaO	4.73	2.52	2.43	5.03	1.46	3.59	1.93	1.43	7.25	7.07	7.29	8.49	2.47
Na ₂ O	3.98	4.19	3.90	3.40	4.09	3.37	3.96	4.07	2.39	2.76	2.79	2.36	4.26
K ₂ O	0.89	2.47	2.81	1.76	2.50	3.15	2.53	3.11	1.61	2.18	2.23	2.03	2.09
P ₂ O ₅	0.17	0.08	0.02	0.17	0.03	0.06	0.06	0.02	0.13	0.12	0.13	0.09	0.08
L.O.I	2.07	1.55	4.95	3.89	1.44	3.20	2.01	1.39	6.84	8.08	6.68	6.72	2.51
Zr	134.545	117.519	77.11	114.205	92.154	121.429	141.781	95.541	66.156	75.547	76.008	67.056	177.51
Total	100.95	100.47	100.85	100.81	99.19	101.01	101.14	101.99	100.70	101.49	100.07	100.48	100.48
Oxide (wt%)	K1 ^{\$}	K2 ^{&}	K3 [%]	K4 ^{\$}	K5 ^{\$}	K6 [%]	K7 ^{\$}	K88 [#]	K87 [#]	4-6 ^{\$}	4-4 ^{\$}	4-1 ^{\$}	3B-4 ^{\$}
SiO ₂	74.98	59.06	49.42	62.12	63.16	49.44	70.49	58.61	72.12	61.65	62.57	54.00	61.76
TiO ₂	0.11	0.62	0.60	0.60	0.64	0.62	0.15	0.77	0.34	0.63	0.68	0.88	0.62
Al ₂ O ₃	12.81	15.73	15.88	17.00	16.73	17.66	13.41	16.74	14.11	16.49	16.51	17.97	15.56
FeO*	1.36	5.03	6.11	4.18	4.22	5.82	1.33	6.43	2.77	4.58	4.48	6.48	4.45
MnO	0.03	0.11	0.14	0.08	0.08	0.13	0.04	0.15	0.05	0.10	0.09	0.15	0.08
MgO	0.30	3.88	6.29	1.79	1.78	5.69	0.70	3.54	0.75	2.20	2.06	3.71	2.11
CaO	1.93	5.78	8.51	4.29	4.56	7.33	3.99	6.06	2.56	5.28	5.25	7.11	5.08
Na ₂ O	4.05	2.86	1.98	3.53	3.90	1.74	3.56	3.07	3.23	3.19	3.50	3.38	3.13
K ₂ O	2.12	1.41	1.80	2.23	1.91	2.68	2.13	1.42	2.81	1.54	1.16	0.92	2.07
P ₂ O ₅	0.04	0.12	0.12	0.16	0.16	0.09	0.05	0.17	0.09	0.15	0.17	0.17	0.15
L.O.I	2.27	5.40	9.15	4.02	2.85	8.79	4.14	3.05	1.17	4.19	3.53	5.24	5.00
Zr	100.969	94.352	75.156	122.799	123.296	71.647	106.766	133.586	175.7	111.26	135.92	104.55	115.46
Total	102.42	101.41	101.02	100.51	100.97	101.40	101.56	100.01	99.65	101.46	101.25	101.28	101.63
Oxide (wt%)	3B-2 ^{\$}	2C-5 ^{\$}	2C-3 ^{\$}	2C-1 ^{\$}	2B-1 ^{\$}	2A-3 ^{\$}	2A-1 ^{\$}	1B-2 ^{\$}	1A-3 ^{\$}	1A-1 ^{\$}			
SiO ₂	60.30	58.43	61.63	58.92	56.23	58.51	59.05	64.58	63.18	64.05			
TiO ₂	0.68	0.79	0.59	0.70	0.79	0.75	0.74	0.57	0.54	0.57			
Al ₂ O ₃	15.73	17.72	16.58	16.10	16.81	15.71	16.50	15.61	15.99	16.47			
FeO*	5.23	5.40	4.15	5.14	6.34	5.74	5.71	3.90	3.74	3.81			
MnO	0.09	0.11	0.08	0.11	0.14	0.14	0.13	0.08	0.08	0.08			

Oxide (wt%)	3B-2 [#]	2C-5 [§]	2C-3 [§]	2C-1 [§]	2B-1 [§]	2A-3 [§]	2A-1 [§]	1B-2 [§]	1A-3 [§]	1A-1 [§]
MgO	2.49	2.40	1.90	2.33	2.91	2.71	2.76	1.67	1.61	1.64
CaO	4.79	3.91	4.09	5.15	5.31	5.07	4.53	4.59	5.22	4.29
Na ₂ O	3.06	3.61	3.39	3.93	3.11	3.10	3.37	3.79	3.87	3.77
K ₂ O	2.27	2.68	2.68	1.93	2.29	2.22	2.01	1.45	1.50	1.62
P ₂ O ₅	0.16	0.19	0.14	0.17	0.17	0.17	0.16	0.14	0.14	0.14
L.O.I	5.20	4.76	4.77	5.51	5.91	5.90	5.04	3.61	4.13	3.56
Zr	121.53	138.35	123.87	118.34	117.95	117.17	105.65	114.16	116.39	114.16
Total	100.72	101.45	101.60	101.08	101.31	101.32	101.81	101.59	100.97	101.62

Table 2. Results for bulk rock compositions determined with the X-ray fluorescence analysis in the cataclasite samples. Degree of cataclasis: #, very weak; §, weak; %, moderate; &, strong.

SiO₂ wt.% greatly varies with increasing degree of cataclasis. First, it increases from 58.6 to 72.1 wt.% in the very weakly fractured rocks to 54.0–76.4 wt.% in the weakly fractured rocks, and then decreases to 49.4–62.8 wt.% and 50.2–59.1 wt.% in the moderately and strongly fractured rocks, respectively (**Table 2**). Associated with this change in SiO₂ wt.%, there is a general tendency that the wt.% of FeO, MgO, and CaO first decreases from the very weakly to weakly fractured rocks, and then increases from the weakly to the moderately and strongly fractured rocks. On the other hand, the wt.% of Na₂O and K₂O first increases and then decreases with increasing degree of cataclasis.

As shown in the compositional changes of major elements in the stratigraphic column (**Figure 5**), the compositional changes are quite abrupt at some horizons, in particular, at two horizons where the depth from the surface is 463.0 and 468.5 m, respectively. Perhaps, these sudden changes in the composition of cataclasite, which are also shown for cataclasites along the San Andreas Fault by [24], indicate the fault zone defined by very strong cataclasis and chemical alteration in the whole cataclasite zone.

3.4. Modal composition of minerals in the cataclasite measured by an XRD

Modal composition of minerals in the cataclasite samples is measured by an XRD (**Table 3**). It is generally clear that the modes of minerals constituting the protolith tonalite mylonite such as albite, quartz, K-feldspar, amphibole, and rutile decrease, while those of newly grown minerals, mostly clay and mica minerals (i.e., chlorite and white mica), and calcite, prehnite, and sphene increase with increasing cataclasis in the analyzed cataclasite samples. However, it should be noted that chlorite, which is normally abundant only in the moderately and strongly fractured cataclasite, is already abundant in some of the very weakly fractured samples (W15 and K88), where the mode of quartz is lower and that of plagioclase is higher than the respective modes in the other very weakly fractured samples (W14 and K87).

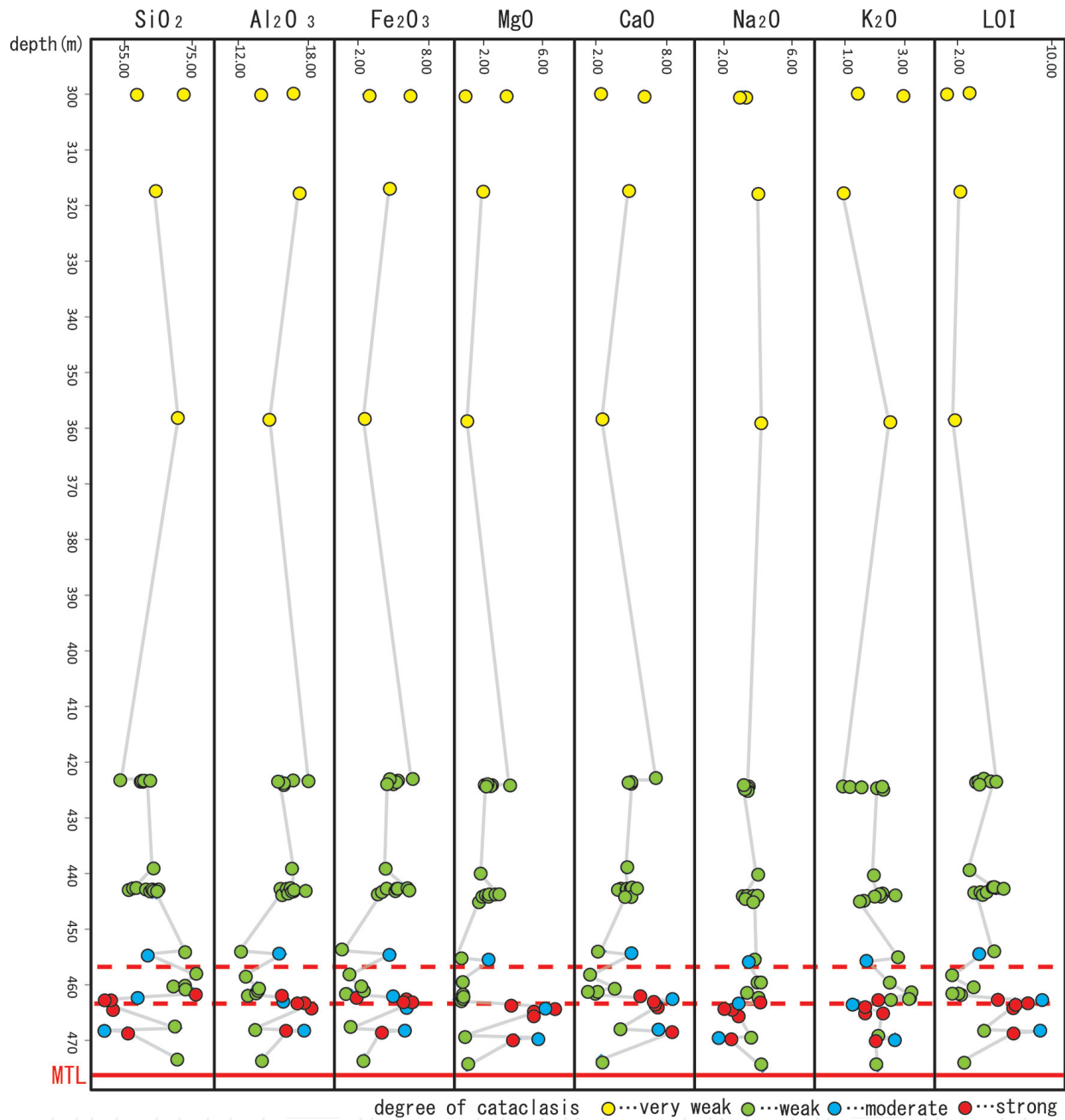


Figure 5. Spatial variation of the bulk rock compositions in the direction of the borehole in the cataclasite samples. Red dashed lines indicate inferred faults.

Therefore, the facts suggest that there are already large variations in the composition of the protolith tonalite mylonite, which could follow their own changes in the modal composition of minerals during cataclasis and alteration. This possibility will be explored in the following section using the principal component analysis (PCA), following which the more refined results of modal composition of minerals in the cataclasite samples will be presented.

Mineral (weight%)	W14	W15	K1	K2	K3	K4	K5	K6	K7	K87	K88
Quartz	34.23	26.75	39.05	27.10	18.86	25.85	24.71	18.29	37.36	36.48	19.70
Kspar	0.00	0.00	0.00	0.00	0.00	0.00	0.00	0.00	0.00	15.97	0.27
Plagioclase	46.85	54.15	37.60	32.93	20.64	43.93	44.01	17.08	32.59	35.74	46.15
Calcite	1.80	1.24	3.24	6.52	12.87	4.32	1.40	12.03	6.23	0.43	1.64
Amphibole	0.00	0.00	0.00	0.00	0.45	0.00	0.00	0.00	0.00	0.00	3.06
Pyrite	0.00	0.00	0.00	0.11	0.07	0.00	0.16	0.00	0.00	0.06	0.34
Sphene	1.81	0.86	0.29	0.16	0.56	0.00	2.09	0.00	0.00	1.07	1.61
Anatase	0.21	0.41	0.00	0.00	0.00	0.00	0.00	0.00	0.00	0.08	0.00
Rutile	0.24	0.00	0.13	0.00	0.00	0.00	0.16	0.00	0.00	0.44	0.00
Epidote	0.17	0.36	0.34	2.67	1.18	0.00	2.27	0.39	0.00	0.62	1.34
Zircon	0.00	0.00	0.00	0.00	0.00	0.00	0.09	0.00	0.00	0.00	0.00
Chabazite	0.00	0.15	0.09	0.00	0.00	0.00	0.21	0.00	0.00	0.00	0.71
Prehnite	0.69	0.00	0.00	0.69	1.02	0.00	3.21	1.01	0.26	0.81	2.16
Total non-clay and non-mica	86.00	83.92	80.74	70.18	55.65	74.10	78.31	48.80	76.44	91.70	76.98
Kaolinite	0.00	0.44	0.22	0.93	2.19	0.00	0.00	1.76	0.00	0.00	1.48
Muscovite	4.83	1.69	12.12	9.58	13.16	14.28	5.89	19.64	13.73	1.07	0.69
Glauconite	0.08	1.83	1.47	0.00	0.00	0.00	0.00	0.00	1.49	0.00	0.75
Talc	0.00	0.00	0.08	1.76	3.76	0.37	0.00	1.54	0.00	0.00	2.00
Chlorite	5.64	13.02	3.22	18.20	24.06	11.83	13.32	23.61	2.65	6.27	18.64
Smectite	0.00	0.49	0.00	0.00	0.03	0.00	0.00	0.00	0.00	0.00	0.00
Total clay and mica	10.55	17.47	17.11	30.47	43.20	26.48	19.21	46.55	17.87	7.34	23.56
Total	96.55	101.39	97.85	100.65	98.85	100.58	97.52	95.35	94.31	99.04	100.54

Table 3. Results of analyses of modal compositions of minerals measured with an XRD in the cataclasite samples.

4. Interpretation

4.1. Principal component analysis (PCA)

In order to investigate why the amount of these chemical elements varies in the cataclasite samples, we have conducted the principal component analysis (PCA) using the free software Easy PCA [15] for the bulk chemical compositions determined for the samples W1, 2, 4, 5, 6, 7, 8, 9, 10, 12, 13, 14, and 15 and K1, 2, 3, 4, 5, 6, 7, 87, and 88. Based on the results of PCA, it has been found that the contribution rates of the first and second principal components are 76 and 15%, respectively, the sum of which exceeds 90%. Hence, only the first and second principal components are considered to interpret the net results. The calculation of factor loadings shows that for the first principal component all the chemical compositions have a similar value, and SiO₂, Na₂O, and K₂O, and the other chemical compositions show opposite sign for

the contribution to the first principal component (**Figure 6a**). On the other hand, for the second principal component, Na_2O , K_2O , P_2O_5 and LOI (loss of ignition) have larger factor loadings than the other chemical compositions, and hence greatly contribute to it (**Figure 6b**). It should be noted that the second principal component increases with the increasing amount of K_2O , while it decreases with the increasing amount of Na_2O . Finally, the values of the first and second principal components of the analyzed bulk chemical compositions from the cataclasite samples with the different fracture densities are plotted in the X-Y coordinates, where the horizontal and vertical axes show the values of first and second principal components, respectively (**Figure 7**). According to this diagram, it has been found that for those samples where the values of the second principal component are mostly positive and greater than -0.1 , the values of the first principal component decrease with increasing fracture density, although the very weakly and weakly fractured, and moderately and strongly fractured samples cannot be distinguished in terms of the value of the first principal component, respectively. This group

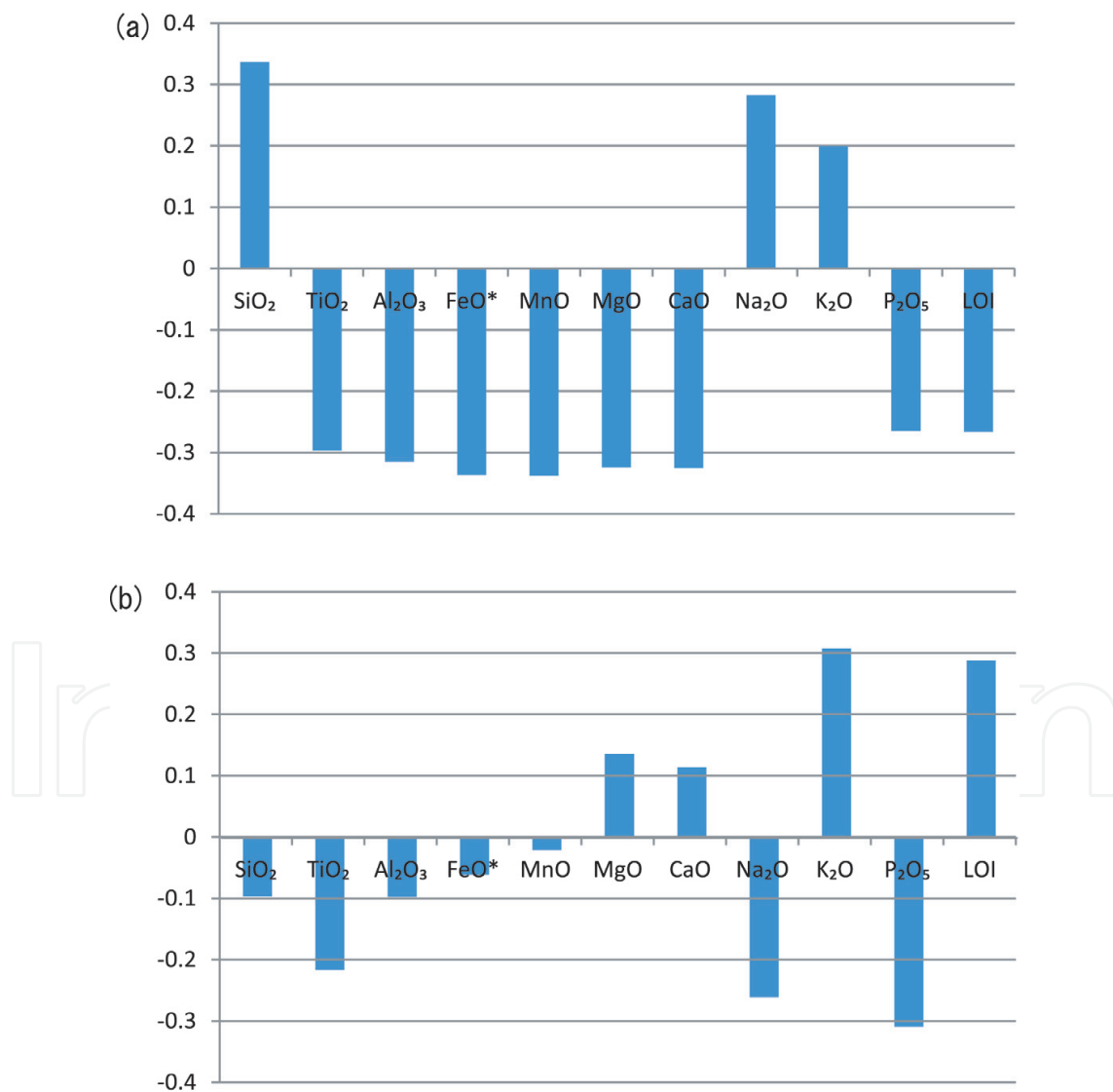


Figure 6. Principal component analysis. (a) Factor loading for the first principal component and (b) factor loading for the second principal component.

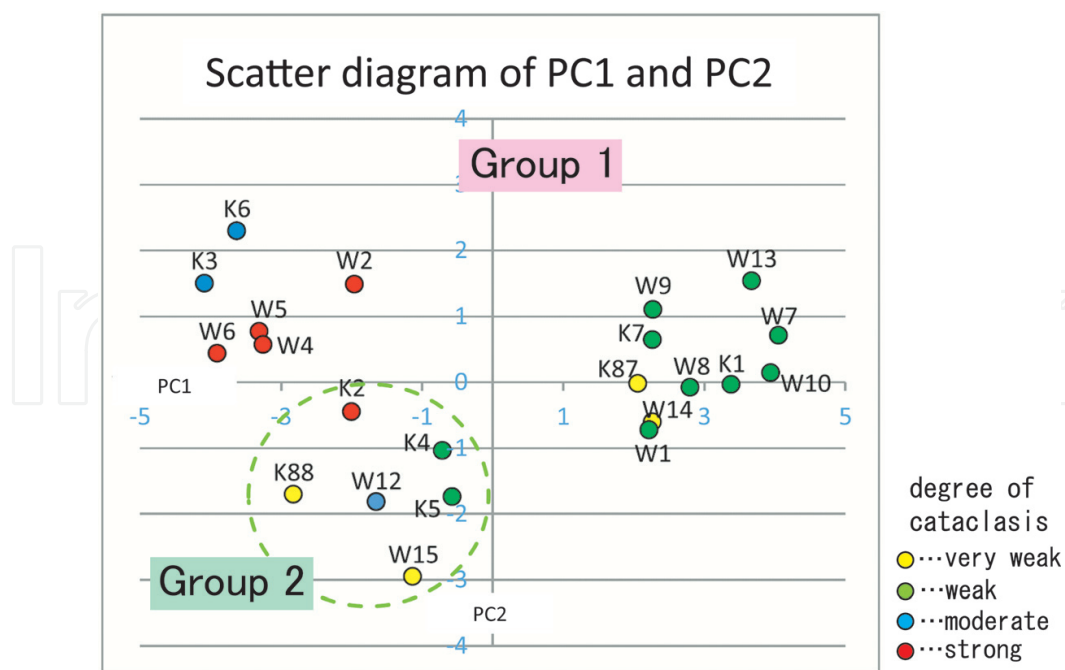


Figure 7. Plots of the first and second principal component values in the X-Y coordinates.

of samples is called Group 1. On the other hands, the plots of those samples where the values of the second principal component are mostly negative and smaller than -1.0 except for K2 are clustered, and they are grouped into Group 2 here.

We have now plotted the modal composition of minerals determined with an XRD analysis in the cataclasite samples K1, K2, K3, K4, K5, K6, K7, K87, K88, and W14 and W15 as a function of fracture densities separately for Group 1 and 2 to interpret the principal components (Figure 8). From this figure, it should be first noted that K-feldspar is only contained in one of the very weakly fractured samples of Group 1 (K87). It should be also noted that the amount of quartz in the very weakly fractured samples is higher in Group 1 than Group 2 sample, while the amount of plagioclase in them is higher in Group 2 than Group 1 sample. These results are consistent with the results of principal component analysis that the second principal component increases with increasing amount of K_2O (major component of K-feldspar) toward Group 1, while it decreases with increasing amount of Na_2O (major component of plagioclase) toward Group 2. The amount of muscovite increases with increasing degree of fracturing for both Groups of samples. The amount of chlorite increases with increasing degree of fracturing in Group 1 samples, while it shows a constant and high value in the very weakly to strongly fractured samples in Group 2 samples. Finally, the amount of calcite increases with increasing degree of fracturing in the cataclasite samples for both Groups.

It has now become clear that the difference between Groups 1 and 2 can be attributed to the difference in modal composition of minerals constituting the protolith. Group 1 samples are derived from more felsic, while Group 2 samples are derived from more mafic protoliths. The interpretation is consistent with the fact that these cataclasite samples from Group 2 contain a large amount of chlorite even at the initial stage of fracturing (in the very weakly and weakly

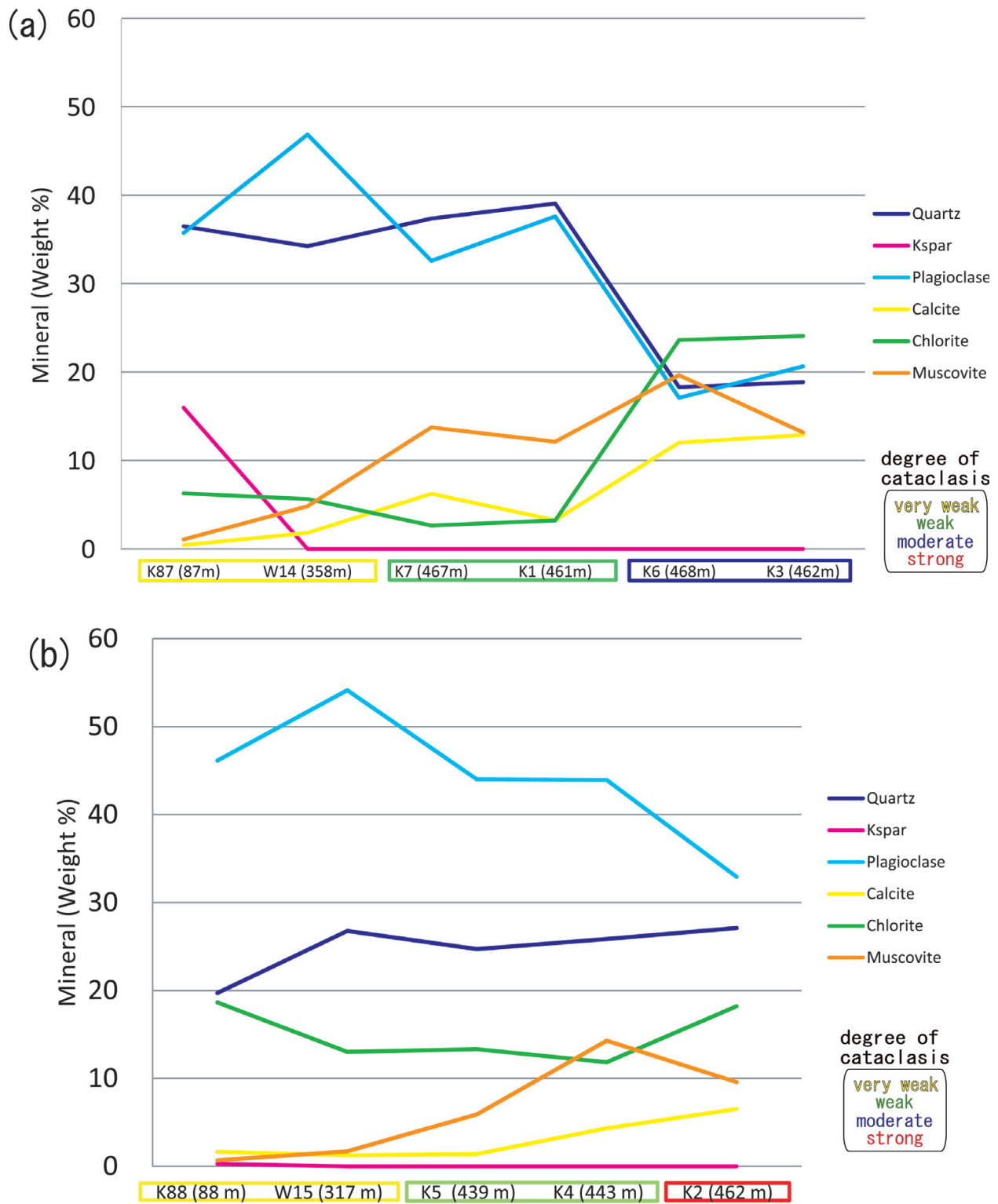


Figure 8. Plots of modal compositions of minerals with increasing fracture densities measured with an XRD in the cataclasite samples. (a) Group 1 and (2) group 2.

fractured samples), which is in accord with the fact that a large amount of biotite and amphibole altered to chlorite is observed in the cataclasite samples W15, K4, K5, and K88 belonging to Group 2 under an optical microscope. Therefore, the second principal component represents

the difference in protolith (i.e., mafic vs. felsic). On the other hand, the value of the first principal component for Group 1 samples changes with changing fracture densities. Therefore, the first principal component perhaps represents the degree of element migration via fluid (i.e., dissolution and precipitation), which is essentially controlled by the fracture densities in the cataclasite samples. The inference is consistent with the facts that while the modal ratios of plagioclase and quartz clasts gradually decrease due to dissolution, those of muscovite and chlorite increase due to precipitation with the increasing density of fractures for Group 1 samples.

4.2. Isocon diagram

In order to analyze the mass changes with increasing cataclasis, we applied the isocon method by [14]. In the isocon diagram, the mass of each major chemical element in the protolith (X) and cataclasite (Y) is plotted as a point in the X - Y coordinate. If there is no mass change in the cataclasite and transfer for any particular chemical element during cataclasis, the slope of the straight line connecting the point (X, Y) and origin is 1. However, the slope is not 1 for most of the chemical elements, which is changed by both mass change in the cataclasite and mass transfer for any particular element during cataclasis. First, we will analyze the mass change during cataclasis based on the slope of the straight line for an immobile element (i.e., immobile isocon). If the slope is less than 1, mass is inferred to increase (i.e., the concentration is decreased). On the other hand, if the slope is more than 1, mass is inferred to decrease (i.e., the concentration is increased). Further, if there is no change in density of rocks, this mass increase or decrease can be treated as volume increase or decrease. In this paper, the mass increase or decrease is rephrased as volume increase or decrease assuming no density change in the cataclasite samples. These mass increase and decrease can be expressed using the slope of immobile isocon (S) by the following equation.

$$\text{Mass increase} = \left[\left(\frac{1}{S} \right) - 1 \right] \quad (1)$$

In this analysis, we use Zr as an immobile element (e.g., see [25]), because at the temperature conditions (<300°C) where the cataclasite samples experienced chemical reactions via fluids, it is considered that zircon cannot be dissolved into fluids [26]. In this study, although we measure the weight percents of other trace elements, we only plot the ones of ZrO_2 and TiO_2 determined by the XRF analysis. Further, the mass transfer of any particular chemical element can be inferred by comparing the slope of straight line for any particular element with that of the immobile isocon. If the slope for any particular element is larger than that of the immobile isocon, the element flows into the system and its mass increases. On the other hand, if the slope for any particular element is smaller than that of the immobile isocon, the element flows out the system and its mass decreases.

In the present study, we have analyzed the mass change and transfer for the following three cases: the very weakly versus weakly fractured samples, the weakly versus moderately fractured samples, the weakly versus strongly fractured samples (**Figure 9**). Since both moderately and strongly fractured samples show the same trend in terms of the mass change and transfer relative to the weakly fractured samples as mentioned below, both chemical compositions are compared with those of the weakly fractured samples. From these analyses, it has been

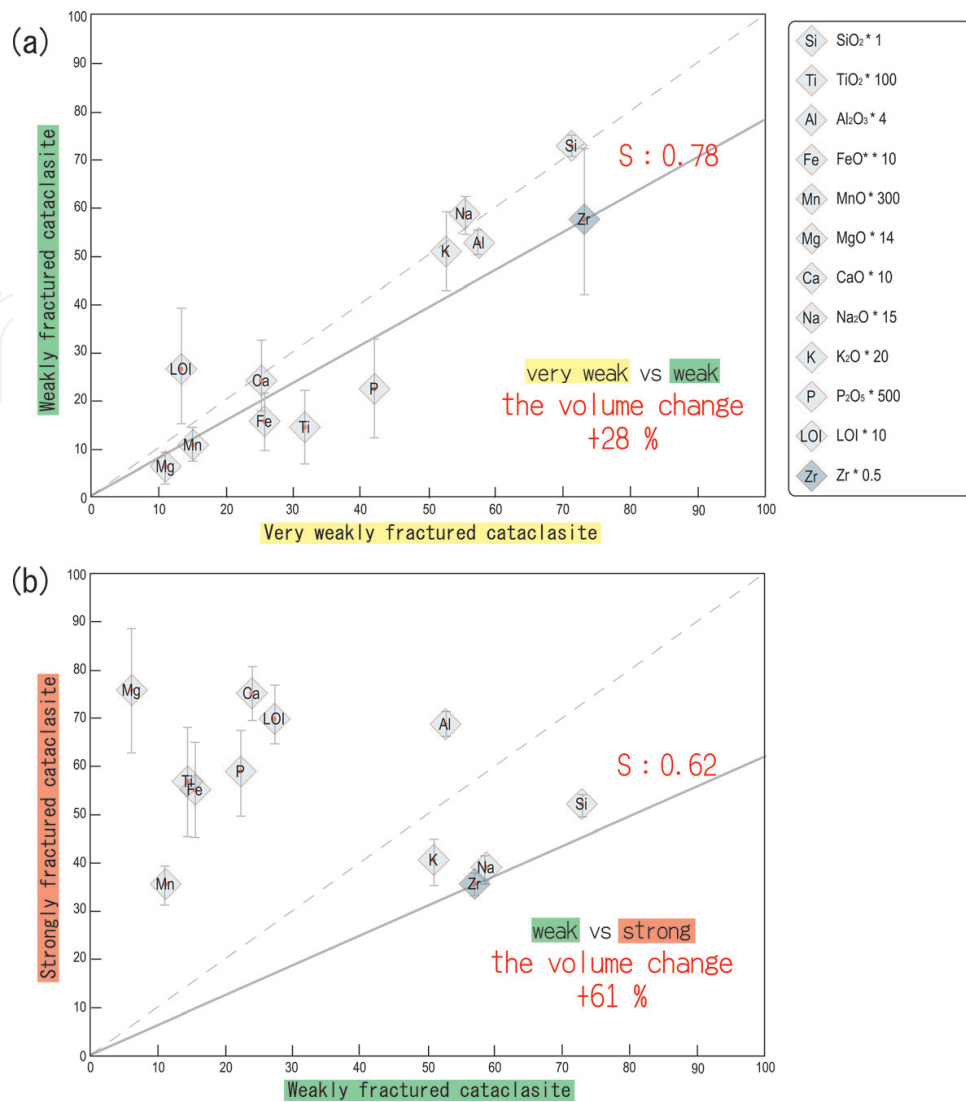


Figure 9. Isocon diagram for the Group 1 cataclasite samples with different degree of cataclasis. (a) Very weakly versus weakly fractured, and (b) weakly versus strongly fractured samples. The isocon diagram for weakly versus moderately fractured samples is not shown.

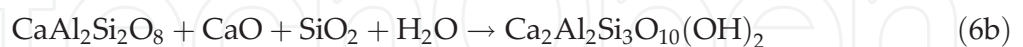
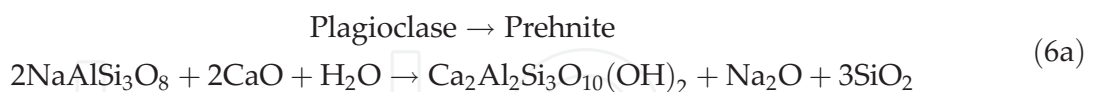
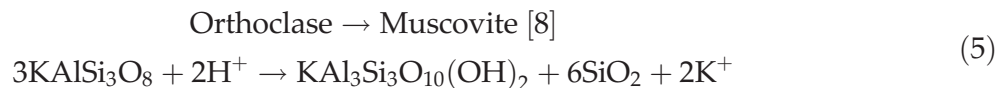
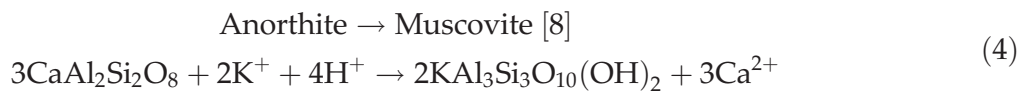
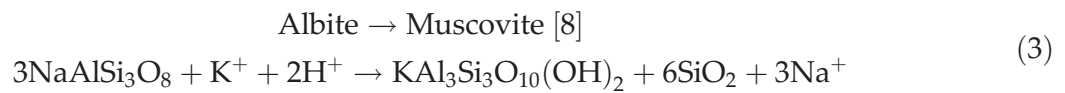
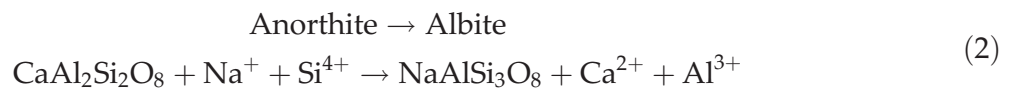
inferred that there is 28% mass increase from the very weakly to weakly fractured samples during cataclasis. Further, there could be 56 and 61% mass increase from the weakly to moderately and strongly fractured samples, respectively.

For the element transfer, from the very weakly to weakly fractured rocks the weight percents of SiO_2 , Na_2O , K_2O , Al_2O_3 , and LOI increase, while those of TiO_2 , FeO^* , MnO , MgO , and CaO decrease (**Figure 9a**). The increase of K_2O can be interpreted by alteration of plagioclase to white mica, which is evidenced by both microstructural observations with a SEM-EDS (**Figure 4**) and modal analysis of constitutive minerals by an XRD (**Figure 8**) in the differently fractured cataclasite samples. The increase of white mica is accompanied by the increase of LOI. The increase of SiO_2 is caused by the formation of quartz veins, which are observed in both core samples and thin sections. The increase of Na_2O is perhaps caused by the formation of albite from oligoclase constituting the protolith tonalite partly mylonitized, which is not completely albitized.

From the weakly to moderately and strongly fractured rocks, the weight percents of FeO*, MgO, CaO, TiO₂, MnO, Al₂O₃, and LOI increase, while those of SiO₂, Na₂O and K₂O are nearly constant (**Figure 9b**). This is interpreted by both further alteration of albite and increase of volume fraction of the ultracataclasite, where the rocks are not only comminuted, but also new minerals precipitated from the solution in the open space formed by fracturing. The increase of CaO is interpreted by not only the precipitation of laumontite and sphene in the ultracataclasite part, but also the replacement of albite by prehnite. The increase of FeO* is interpreted by the precipitation of chlorite and iron sulfide (e.g., pyrite). The increase of MgO, MnO, and LOI is interpreted by the precipitation of chlorite, that of Al₂O₃ by the precipitation of chlorite and laumontite, and that of TiO₂ by the precipitation of sphene from rutile (**Figure 4**) in the ultracataclasite part.

4.3. Dissolution and precipitation reaction of minerals via fluids in the cataclasite

Based on the identification of minerals in plagioclase porphyroclast and ultracataclasite, the analyses of change of modal composition of minerals with an XRD and mass transfer using isocon diagrams with increasing cataclasis, we have inferred that the following dissolution and precipitation reactions occurred via fluids during cataclasis in the analyzed samples.



5. Discussion

5.1. Two-stage mass transfer during cataclasis

As mentioned earlier, two-stage mass transfer during cataclasis could be identified based on the isocon diagrams in the analyzed cataclasite samples. The elements analyzed can be divided into three groups from the viewpoint of mass transfer: SiO₂, Na₂O, and K₂O (the first group of elements), which increase at the first stage, and then do not change very much at the second stage; FeO*, MgO, CaO, TiO₂, and MnO (the second group of elements) which decrease at first

stage, and then increase at the second stage; Al_2O_3 and LOI which increase at both stages. Here, the first stage denotes the cataclasis from the very weakly to weakly fractured cataclasites, and the second stage that from the weakly to moderately and strongly fractured cataclasites. This kind of two-stage mass transfer was also observed for the cataclasites derived from leucogranite, where K-feldspar is abundant [8], although the trend of mass transfer is different for some elements between the cataclasites originated from leucogranite and tonalite analyzed in the present study. In the case of the cataclasites derived from leucogranite, K_2O decreases during the cataclasis from leucogranite to ultracataclasite (first stage), and then increases from ultracataclasite to fault phyllonites (second stage), while CaO increases at the first stage, and then decrease at the second stage. For other elements, the trend of mass transfer at both stages is similar to that of the present case. The difference in the trend of mass transfer between the leucogranite and tonalite protoliths results from the facts that for the case of leucogranite protolith the clay mineral ultimately formed is muscovite, while for the case of tonalite the clay mineral ultimately formed is chlorite, and Ca-phases such as prehnite, laumontite, sphene, calcite are abundant in the moderately and strongly fractured rocks. However, the two-stage alteration and mass transfer for both cases could imply that mass transfer is internally balanced (cf. [27]), so that the first group of elements (CaO belongs to the first group, while K_2O belongs to the second group for the case of leucogranite protolith) migrated from the moderately and strongly fractured cataclasites to the weakly fractured cataclasites, while vice versa for the second group of elements. On the other hand, a large amount of mass increase is inferred in the cataclasite zone as a whole, and hence the mass transfer from the outside of the system is not precluded as mentioned in the subsequent text.

5.2. A large mass increase during cataclasis

In the present study, it has been inferred that there is 28% mass increase from the very weakly to weakly fractured samples during cataclasis. Further, there could be 56 and 61% mass increase from the weakly to moderately and strongly fractured samples, respectively. So, considering that the strongly fractured samples are derived from the weakly fractured samples, which themselves are derived from the very weakly fractured sample, there could be c. 110% mass increase in the strongly fractured cataclasite samples caused by mass transfer, which occurred during the entire period of fracturing. The origin of this large amount of mass increase in the cataclasite samples will be discussed in the subsequent text.

First of all, the inference of mass changes is greatly dependent on the selection of immobile elements. In the present study, although we select Zr as an immobile element, other studies used Ti [28], both Ti and Zr [24, 27] as immobile elements, or take the average slope of isocons of relatively immobile elements for the slope of immobile isocon [29]. However, we did not use Ti as an immobile element because a large amount of sphene is grown from rutile by chemical reaction aided by the presence of fluids. In fact, the slopes of isocons of TiO_2 and ZrO_2 are greatly different. However, if we take the average slope of isocons of relatively immobile elements as the slope of immobile isocon, the present results could be greatly modified. We currently do not know how we should choose an immobile element or how we could infer the slope of isocon of immobile element. Hence, the mass change in the cataclasite samples during cataclasis remains to be investigated.

Nevertheless, we will discuss the origin of this large volume increase in the present cataclasite sample, referring to previous studies. Most of the studies on the volume changes caused by mass transfer during cataclasis reported a significant amount of volume loss for granite protolith ($37 \pm 10\%$ volume loss, see, e.g., [28]). This is reasonable because a large amount of silica dissolved from quartz into fluids by pressure solution is expelled from cataclasites. In fact, microstructures such as solution seams indicating pressure solution are ubiquitous in the present cataclasites. However, a few studies indicate a significant amount of volume increase for granite protolith [27] and for protolith of mafic igneous rocks (gabbro) [29]. Ref. [27] argues that the volume change in phyllonite zones is so valuable ranging between -35 and $+95\%$ at a meter scale in the extensional stress field. Ref. [29] argues that extension fractures in hard rocks such as metabasite are sustained yielding volume increase, while these are easily compressed in soft rocks such as paragneiss yielding volume decrease caused by mass transfer during cataclasis. For the present case of tonalite protolith, since the strength could be between those of granite and gabbro, the volume loss could have been prohibited due to the relatively high strength. Also, the tectonic setting such as extensional stress field, which has not been fully known, may have favored the significant amount of volume increase in the cataclasites. However, the origin of the significant amount of volume increase inferred in the present study remains to be investigated, including the problem if this estimate of volume change is correct or not.

6. Summary

Based on microstructural, and bulk chemical and microchemical analyses of the cataclasite samples collected from the Median Tectonic Line, Mie Prefecture, southwest Japan, we have summarized the present work as mentioned below. In the present cataclasite samples, the progress of cataclasis, which is quantified by the fracture densities (FD, number/cm), is accompanied by the change in bulk chemical compositions determined by the XRF analysis. Both principal component and isocon analyses for the bulk rock compositions in the cataclasite samples reveal the origin of variation of chemical compositions, which mostly results from two-stage mass transfer during cataclasis. Further, a SEM-EDS analysis of altered plagioclase and ultracataclasite (i.e., fine-grained materials by comminution) and XRD analysis with the aid of "RockJock" software delineate that the mass transfer in these cataclasite samples is indeed caused by dissolution and precipitation of minerals, which occurred during cataclasis.

Acknowledgements

We thank Jun Kameda for assistance with XRD analysis with the aid of "RockJock." This research was supported by MEXT KAKENHI grant 26109004 to TT, NS, and KF. Also, this study was supported by the Joint Usage/Research Center Program of Earthquake Research Institute, The University of Tokyo.

Author details

Yumi Kaneko^{1*}, Toru Takeshita², Yuto Watanabe², Norio Shigematsu³ and Ko-Ichiro Fujimoto⁴

*Address all correspondence to: yumi.kaneko@japex.co.jp

1 Japan Petroleum Exploration Co., Ltd., Tokyo, Japan

2 Hokkaido University, Hokkaido, Japan

3 Advanced Industrial Science and Technology, Tsukuba, Japan

4 Tokyo Gakugei University, Tokyo, Japan

References

- [1] Research Group on active fault. Active Faults in Japan (New Version): Distribution Map and Data. Tokyo: University of Tokyo Press; 1991. p. 440. ISBN:978-4-13-060700-1
- [2] Sagiya T, Miyazaki S, Tada T. Continuous GPS Array and Present-day Crustal Deformation of Japan. *Pure and Applied Geophysics*. 2000;**157**:2303–2322. DOI: 10.1007/PL00022507
- [3] Shimamoto T. Rheology of rocks and plate tectonics—From rigid plate to deformable plate. *Kagaku*. 1989;**59**:170–181 (in Japanese)
- [4] Fousseis F, Handy MR, Schrank C. Networking of shear zones at the brittle-to-viscous transition (Cap de Creus, NE Spain). *Journal of Structural Geology*. 2006;**28**:1228–1243
- [5] Schrank CE, Handy MR, Fousseis F. Multiscaling of shear zones and the evolution of the brittle-to-viscous transition in continental crust. *Journal of Geophysical Research*. 2008;**113**:B01407. DOI: 10.1029/2006JB004833
- [6] Bos B, Spiers CJ. Frictional-viscous flow of phyllosilicate-bearing fault rocks: Microphysical model and implications for crustal strength profiles. *Journal of Geophysical Research*. 2002;**107**:1–13. DOI: org/10.1029/2001JB000301
- [7] Holdsworth RE, van Diggelen EWE, Spiers CJ, de Bresser JHP, Walker RJ, Bowen L. Fault rocks from the SAFOD core samples: Implications for weakening at shallow depths along the San Andreas Fault, California. *Journal of Structural Geology*. 2011;**33**:132–144. DOI: 10.1016/j.jsg.2010.11.010
- [8] Wibberley C. Are feldspar-to-mica reactions necessarily reaction-softening? *Journal of Structural Geology*. 1999;**21**:1219–1227

- [9] Takeshita T, El-Fakharani AH. Coupled micro-faulting and pressure solution creep overprinted on quartz schist deformed by intracrystalline plasticity during exhumation of the Sambagawa metamorphic rocks, southwest Japan. *Journal of Structural Geology*. 2013;**46**:142–157. DOI: 10.1016/j.jsg.2012.09.014
- [10] Misch P. Paracrystalline microboudinage of zoned grains and other criteria for synkinematic growth of metamorphic minerals. *American Journal of Science*. 1969;**267**:43–63
- [11] Shimizu I. Kinetics of pressure solution creep in quartz: Theoretical considerations. *Tectonophysics*. 1995;**245**:121–134
- [12] Shigematsu N, Fujimoto K, Tanaka N, Furuya N, Mori H, Wallis S. Internal structure of the Median Tectonic Line fault zone, SW Japan, revealed by borehole analysis. *Tectonophysics*. 2012;**532–535**:103–118. DOI: 10.1016/j.tecto.2012.01.024
- [13] Eberl DD. User's guide to RockJock—A program for determining quantitative mineralogy from powder X-ray diffraction data. USA: Geological Survey Open-File Report; 2003. p. 47
- [14] Grant JA. The isocon diagram—a simple solution to Gresens' equation for metasomatic alteration. *Economic Geology*. 1986;**81**:1976–1982
- [15] Davis JC. *Statistics and Data Analysis in Geology*. New York: John Wiley and Sons Inc.; 2002. p. 638
- [16] Kubota Y, Takeshita T. Paleocene large-scale normal faulting along the Median Tectonic Line, western Shikoku, Japan. *Island Arc*. 2008;**17**:129–151
- [17] Hara I, Shyoji, K, Sakurai Y, Yokoyama S, Hide K. Origin of the Median Tectonic Line and its initial shape. In: Ichikawa K, editor. *Memoirs of the Geological Society of Japan*. Vol. 18. Tokyo: The Geological Society of Japan; 1980. pp. 27–49
- [18] Sakakibara N. Qualitative estimation of deformation temperature and strain rate from microstructure and lattice preferred orientation in plastically deformed quartz aggregates. *Journal of Geological Society of Japan*. 1996;**102**:199–210
- [19] Shimada K, Takagi H, Osawa H. Geotectonic evolution in transpression regime: Time and space relationships between mylonitization and folding in the southern Ryoke belt, eastern kii Peninsula, southwest Japan. *Journal of Geological Society of Japan*. 1998;**104**:825–844
- [20] Shigematsu N, Otsubo M, Fujimoto K, Nobuaki Tanaka N. Orienting drill core using borehole-wall image correlation analysis. *Journal of Structural Geology*. 2014;**67**:293–299. DOI: [org/10.1016/j.jsg.2014.01.016](http://dx.doi.org/10.1016/j.jsg.2014.01.016)
- [21] Hayama Y, Yamada T, Ito M, Kutsukake T, Masaoka K, Miyakawa K, Mochizuki Y, Nakai Y, Tainosho Y, Yoshida M, Kawarabayashi I, Tsumura Y. Geology of the Ryoke Belt in the eastern Kinki District, Japan—The phase-divisions and the mutual relations of the granitic rocks. *Journal of Geological Society of Japan*. 1982;**88**:451–466

- [22] Hayama Y, Yamada T. Median Tectonic Line at the stage of its origin in relation to plutonism and mylonitization in the Ryoke belt. In: Ichikawa K, editor. *Memoirs of the Geological Society of Japan*. Vol. 18. 1980. pp. 5–26
- [23] Jefferies SP, Holdsworth RE, Wibberley CAJ, Shimamoto T, Spiers CJ, Niemeijer AR, Lloyd GE. The nature and importance of phyllonite development in crustal-scale fault cores: An example from the Median Tectonic Line, Japan. *Journal of Structural Geology*. 2006;**28**:220–235
- [24] Schleicher AM, Tourscher SN, van der Pluijm BA, Warr LN. Constraints on mineralization, fluid-rock interaction, and mass transfer during faulting at 2–3 km depth from the SAFOD drill hole. *Journal of Geophysical Research*. 2009;**114**:(B04202). DOI: 10.1029/2008JB006092
- [25] Grant JA. Isocon analysis: A brief review of the method and applications. *Physics and Chemistry of the Earth*. 2005;**30**:997–1004. DOI: 10.1016/j.pce.2004.11.003
- [26] Harley SL, Kelly NM, Moller A. Zircon behavior and the thermal histories of mountain chains. *Element*. 2007;**3**:25-30
- [27] Hippertt, JF. Breakdown of feldspar, volume gain and lateral mass transfer during mylonitization of granitoid in a low metamorphic grade shear zone. *Journal of Structural Geology*. 1998;**20**:175–193
- [28] Evans JP, Chester FM. Fluid-rock interaction in faults of the San Andreas system: Inferences from San Gabriel fault rock geochemistry and microstructures. *Journal of Geophysical Research*. 1995;**100**:13. DOI: 007-13020
- [29] Zulauf GS, Palm S, Petschick R, Spiers O. Element mobility and volumetric strain in brittle and brittle-viscous shear zones of the superdeep well KTB (Germany). *Chemical Geology*. 1999;**156**:135–149